Experimental Mechanics (2021) 61:159–169
https://doi.org/10.1007/s11340-020-00656-8

SP ISS: EXPERIMENTAL ADVANCES IN CARDIOVASCULAR BIOMECHANICS

In Vivo Image-Based 4D Modeling of Competent and Regurgitant Mitral Valve Dynamics

A.H. Aly[1,2] · A.H. Aly[1] · E.K. Lai[3] · N. Yushkevich[1] · R.H. Stoffers[4] · J.H. Gorman IV[3] · A.T. Cheung[5] · J.H. Gorman III[3] · R.C. Gorman[3] · P.A. Yushkevich[1] · A.M. Pouch[1,2]

Received: 31 January 2020 / Accepted: 5 August 2020 / Published online: 17 August 2020
© Society for Experimental Mechanics 2020

Abstract

Background In vivo characterization of mitral valve dynamics relies on image analysis algorithms that accurately reconstruct valve morphology and motion from clinical images. The goal of such algorithms is to provide patient-specific descriptions of both competent and regurgitant mitral valves, which can be used as input to biomechanical analyses and provide insights into the pathophysiology of diseases like ischemic mitral regurgitation (IMR).

Objective The goal is to generate accurate image-based representations of valve dynamics that visually and quantitatively capture normal and pathological valve function.

Methods We present a novel framework for 4D segmentation and geometric modeling of the mitral valve in real-time 3D echocardiography (rt-3DE), an imaging modality used for pre-operative surgical planning of mitral interventions. The framework integrates groupwise multi-atlas label fusion and template-based medial modeling with Kalman filtering to generate quantitatively descriptive and temporally consistent models of valve dynamics.

Results The algorithm is evaluated on rt-3DE data series from 28 patients: 14 with normal mitral valve morphology and 14 with severe IMR. In these 28 data series that total 613 individual 3DE images, each 3D mitral valve segmentation is validated against manual tracing, and temporal consistency between segmentations is demonstrated.

Conclusions Automated 4D image analysis allows for reliable non-invasive modeling of the mitral valve over the cardiac cycle for comparison of annular and leaflet dynamics in pathological and normal mitral valves. Future studies can apply this algorithm to cardiovascular mechanics applications, including patient-specific strain estimation, fluid dynamics simulation, inverse finite element analysis, and risk stratification for surgical treatment.

Keywords Mitral valve imaging · 4D segmentation · Echocardiography · Mitral regurgitation

Introduction

In-vivo mitral valve strain estimation has historically been performed using surgically implanted localized markers, such as sonomicrometry and radiopaque tantalum markers [1–3]. While these in-vivo techniques have provided valuable insight into mitral valve physiology and pathophysiology particularly in animal models, image-based non-invasive strategies for in-vivo strain estimation are critical to application in humans within a clinical setting. As a response to this challenge, recent studies have described non-invasive techniques for mitral valve strain estimation from real-time 3D echocardiographic (rt-3DE) images [4, 5]. These algorithms are significant steps towards building clinically applicable mitral valve strain assessment tools, but a critical challenge is that they are reliant on image segmentations. Likewise, research in mitral valve

Electronic supplementary material The online version of this article (https://doi.org/10.1007/s11340-020-00656-8) contains supplementary material, which is available to authorized users.

✉ A. M. Pouch
pouch@pennmedicine.upenn.edu

1 Department of Radiology, University of Pennsylvania, Philadelphia, PA, USA

2 Department of Bioengineering, University of Pennsylvania, Philadelphia, PA, USA

3 Gorman Cardiovascular Research Group, Perelman School of Medicine at the University of Pennsylvania, Philadelphia, PA, USA

4 University of Groningen, Groningen, Netherlands

5 Department of Anesthesiology, Perioperative and Pain Medicine, Stanford University Medical Center, Stanford, CA, USA

repair simulation and finite element modeling requires detailed image-derived valve reconstructions [7–11]. Finite element modeling has been used to study valve physiology and related medical device design. Mechanical modeling of the mitral valve relies on assumptions and identification of parameters for constitutive models. The earliest FEM models have assumed an idealized geometry of the mitral valve and have evolved to include more detail derived from patient-specific imaging. Algorithms have also included thickness modeling from computed tomography [6] and require assumptions related to the dynamics of the mitral valve and chordal tension forces. Therefore, the ability to automatically segment and geometrically model the mitral valve from clinical images, especially from rt-3DE which is frequently used in preoperative surgical planning, is essential for implementing mitral valve tissue mechanics analyses for surgical planning and decision making.

Towards this end, several studies have explored 4D mitral valve segmentation and modeling. In [12], the mitral valve is first segmented in a diastolic 3DE image using graph cuts and the resulting mesh evolves under a set of data-driven and regularization forces to capture valve shape in the other images in the series. Application-specific regularization includes forces that tether the leaflet free edges into the left ventricle, enforce a physiological strain on the leaflets, and prevent collision along the leaflet free margin. In [13], a landmark-based deformable model of the mitral and aortic valves is first initialized in two frames in the cardiac cycle. For all other frames, landmark motion is predicted using manifold learning and clustering and then updated by an optical flow tracker and boundary detection. The result is a full 4D surface model of both valves. A drawback of these methods is that they do not generate volumetric segmentations that distinguish the atrial and ventricular surfaces or capture locally varying thickness of the leaflets, which is an important material property in studying valve tissue mechanics [14].

The development of a 4D automated tool that allows for consistent landmarking and modeling of the mitral leaflets can aid in solving clinical dilemmas such as whether to treat ischemic mitral regurgitation with repair or replacement. Ischemic mitral regurgitation (IMR) is a condition in which the mitral valve becomes incompetent due to ischemic disease of the left ventricle. Transesophageal rt-3DE is the standard of care for preoperative assessment of IMR in many major medical centers. Given the high recurrence rate of moderate to severe IMR after valve repair surgery (33% in the first year [15]), there is a great need to identify patients at elevated risk of recurrence, for whom alternative surgical approaches (complete valve replacement) may provide better long-term outcomes. Recently, 3D morphological features extracted from intra-operative rt-3DE of the diseased valve were shown to predict post-repair IMR recurrence [16]. Static features, such as leaflet tethering angles, have demonstrated promising predictive value but only take advantage of rt-3DE data at a single phase of the cardiac cycle. Since the etiology of IMR is functional left ventricular disease, it is likely that features of mitral valve *dynamics* could potentially bolster recurrence prediction. Towards this end, we have developed an automated spatiotemporal image analysis algorithm that can be used to quantitatively describe mitral valve shape and motion in normal and IMR subjects.

In this work, we build upon the work presented in [17] and present a 4D segmentation method that combines the benefits of atlas-based segmentation and deformable modeling with medial axis-based representation, which produces topologically consistent *volumetric models* of the mitral valve. The former uses expert knowledge of valve image appearance to label the target rt-3DE series and the latter establishes geometric correspondences across subjects and facilitates statistical shape analysis. Temporal coherence is enforced in the segmentation stage by employing a groupwise implementation of multi-atlas label fusion, which updates segmentations of individual 3DE frames using information from its temporal neighbors in the same image series. Temporal consistency is also enforced during the modeling phase by using the Kalman filter to smooth the trajectories of deformable models fitted to the label fusion results. In contrast to previous work [12, 13], this method is validated against label maps of the valve at every frame in the rt-3DE series. Moreover, it demonstrates the ability to compare functional valve measurements in subjects with normal mitral valve function and in subjects with severe IMR.

Materials and Methods

Image Data and Manual Segmentation

The iE33 imaging platform (Philips Medical Systems, Andover, MA) was used to acquire ECG-gated rt-3DE images of the mitral valve from 28 patients: 14 with normal mitral valve structure and function and 14 with severe IMR. Images were obtained over four consecutive cardiac cycles with a 2–7 MHz matrix-array transesophageal transducer. The rt-3DE acquisitions over consecutive cardiac cycles were obtained at end-expiration during positive pressure ventilation in anesthetized patients to eliminate motion caused by respiration. Each subject's rt-3DE image series consisted of 10–37 frames (temporal resolution of 18–40 Hz) showing the mitral valve over one cardiac cycle beginning at early systole. The images were exported in Cartesian format with nearly isotropic resolution ranging from 0.4 to 0.8 mm. All data series, totaling 613 individual 3DE images, were manually segmented in ITK-SNAP, an interactive medical image segmentation tool [18]. An expert observer separately labeled the anterior and posterior leaflets in each 3DE image. The manual segmentations

served as atlases for multi-atlas label fusion and as references for cross-validation of automated segmentation.

Automated Image Analysis

Automated 4D mitral valve segmentation requires a reference atlas set consisting of manually traced images at each phase of the cardiac cycle, and a deformable model of the valve. The only manual interaction required to segment a new unseen target image series is the identification of several temporal and physical landmarks in the target series, described below. First, the series is segmented using a groupwise implementation of multi-atlas label fusion. Then, a mitral valve model in the form of a medial axis representation is deformed to the groupwise segmentation result with enforcement of temporal coherence. The combination of these techniques facilitates standardized automated measurements of mitral valve dynamics in rt-3DE data. Figure 1 illustrates an overview of this pipeline and Figs. 2, 3 and 4 demonstrate the specifics of each step of the pipeline.

Cardiac Phase Detection and Landmark Initialization Given an unseen target rt-3DE image series to segment, a user first identifies two frames in the cardiac cycle: mid-systole and mitral valve opening. As illustrated in Fig. 2, the user identifies five landmarks in the mid-systolic image: the anterior aortic peak of the annulus, two commissures, the midpoint of the coaptation line, and the midpoint of the posterior annulus. The purpose of the landmarks is to roughly initialize the affine transformation needed to align the atlas and target images. Because the utility of landmarking is used for rough initialization rather than for final measurements, inter-user variability does not likely have a strong impact on the final patient-specific geometric model, especially if the landmarks are within several millimeters [19]. Similar approaches to initialization using either automated landmarking or manual tracing have been used in other valve segmentation tools [12, 13, 20]. While it may be possible to automate this step using convolutional and recurrent neural networks as in [21], which applies to landmark magnetic resonance imaging data sets, it requires a much larger dataset especially for echocardiography where the contrast is not as high.

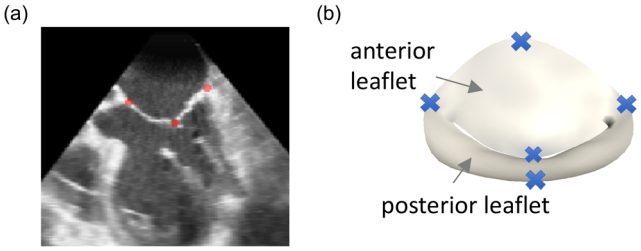

Fig. 2 **a** Example of landmarking in a cross-section of a 3DE image, from left to right: midpoint of posterior annulus, midpoint of the coaptation line, and the anterior aortic peak of annulus. **b** Anatomical representation of five manually identified mitral valve landmarks, from top to bottom: anterior aortic peak of the annulus, two commissures, the midpoint of the coaptation line, and the midpoint of the posterior annulus

Intra-subject registrations The spatial landmarks identified in the mid-systolic frame are first propagated to the other frames in the rt-3DE series in order to accurately initialize multi-atlas segmentation of each individual frame. Landmark propagation is achieved by deformable registration between pairs of 3D images within the target image series. Figure 3 illustrates that all pairs of images within the same phase of the cardiac cycle are registered to one another, both for landmark propagation and for groupwise multi-atlas segmentation as described below. In addition to these intra-phase registrations, the mid-systole frame is registered to the mid-diastole frame, and the mid-diastole frame is registered to the transitional frame (i.e., mitral valve opening). This allows for the mid-systole landmarks to be propagated to all frames within the target rt-3DE image series. The intra-subject registrations also facilitate groupwise iterations of multi-atlas segmentation as described below. All deformable registrations are performed with the open-source Advanced Normalization Tools (ANTs) toolkit [22].

Groupwise Multi-Atlas Segmentation Given the relatively small number of cases and the consistency in mitral valve appearance in 3D TEE, we take advantage of multi-atlas label fusion (MALF) [23] as an alternative to machine learning

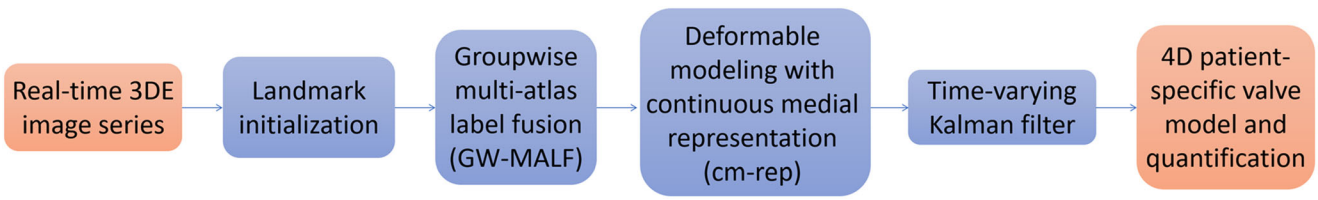

Fig. 1 Summary of the image analysis pipeline for automatic segmentation and modeling. The user identifies 2 temporal landmarks and 5 spatial landmarks. Groupwise multi-atlas label fusion is used to generate temporally coherent segmentations of all frames in an image series. Deformable continuous medial representation (cm-rep) is then used to generate topologically consistent volumetric models of the mitral valve from the segmentation results. Temporal consistency is enforced with a Kalman filter. The final output is a 4D patient-specific mitral valve model that can be used for shape analysis

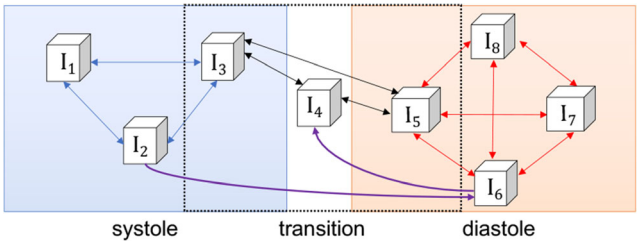

Fig. 3 Intra- and inter-cardiac phase registration within the target image series. Intra-phase registrations: all pairs of 3D images within a cardiac phase are registered to each other. Inter-phase registrations: mid-systolic frame $\boldsymbol{I_2}$ is registered to the mid-diastole frame $\boldsymbol{I_6}$, which is registered to the transitional frame $\boldsymbol{I_4}$

techniques that require very large training data sets**.** Multi-atlas label fusion (MALF) uses a set of expert-labeled images, referred to as atlases, to generate individual candidate segmentations of a target image. Each candidate segmentation is created by performing deformable registration between the target and atlas image, and then warping the atlas labels to the target image space. Registration is initialized with the user-identified landmarks described above. Since the candidate segmentations may not be accurate on their own, they are merged into a higher quality segmentation using a consensus-seeking strategy called label fusion, which uses spatially varying intensity-based weighted voting to combine the candidates into a consensus label map [24]. In order to extend 3D MALF to the spatiotemporal domain, we use a *groupwise* adaptation of MALF [25]. First, each 3DE image in the series is

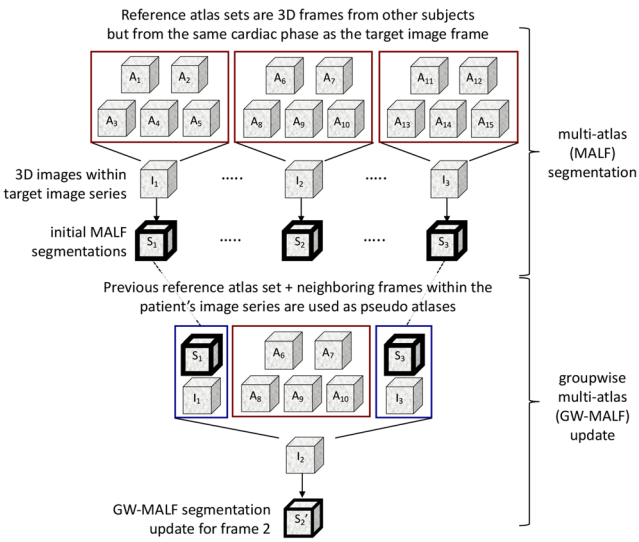

Fig. 4 Summary of groupwise multi-atlas label fusion. A set of reference 3D images is assigned to each frame within a target image series. Multi-atlas joint label fusion is performed independently on each 3DE image in the series. The multi-atlas segmentations are then iteratively updated using the image's temporal neighbors as pseudo-atlases, in addition to the initially assigned reference images. An example of a groupwise segmentation update for frame 2 is shown. Here, *I* denotes a 3D image within the target series, *S* denotes a 3D segmentation, and *A* denotes a 3D atlas from other subjects' data sets. The numbered subscripts indicate frame numbers

independently segmented with MALF using other subjects' atlases. Once an initial segmentation is generated for each frame, the series of segmentations is iteratively updated using both the original reference atlases and the MALF segmentations of neighboring 3DE images as "pseudo" reference atlases. By weighting the "pseudo" atlases equal to or more than the original atlas set, the iteratively updated segmentations become more coherent with one another, capturing the similarity in the segmentations of the same structure moving over time.

A challenge of using groupwise MALF (GW-MALF) for 4D valve segmentation is that performing within-subject deformable registration between the valve at systole and diastole often produces poor results because the temporal resolution of image acquisition is not sufficient to provide many intermediate images of the leaflets during rapid valve opening. To overcome this challenge, GW-MALF is performed separately in overlapping cardiac phases: systole, transition, and diastole. Figure 4 illustrates that for each 3D image I_n in a sample target series, a set of atlases $\{A_f^s\}$ is selected from the same cardiac phase and a neighboring cardiac phase of other subjects' data sets. Each 3DE image I_n in the target series then has an independent atlas set $\{A_f^s\}$. Here, f denotes a set of frame numbers and s denotes a set of subject identifiers. In the first round of MALF, each I_n is segmented using only the reference atlas set $\{A_f^s\}$. In the subsequent groupwise iterations, the segmentation of I_n is updated using the segmentations of I_{n-1} and I_{n+1} as pseudo atlases, along with the original atlas set $\{A_f^s\}$.

Deformable Medial Modeling Once a series of valve segmentations is obtained, a deformable model in the form of a continuous medial representation (cm-rep) [26] is warped to the GW-MALF results. This step imposes a fixed topology on the final segmentation, establishes correspondences on different patients' segmentations, and facilitates automated morphological measurement. An advantage of combining label fusion and deformable medial modeling is that medial modeling can geometrically correct segmentation artifacts such as holes and over-segmentation. Cm-rep describes the valve in terms of its medial axis geometry and is parameterized by $\{\mathbf{m}, R\} \in \mathbb{R}^3 \times \mathbb{R}^+$, where $\mathbf{m}$ is a continuous medial manifold and R is a radial thickness field defined over the medial manifold. Numerically, the medial manifold and leaflet surfaces are represented by triangulated meshes that can be sequentially Loop subdivided to a desired vertex density. The template medial mesh, shown in Fig. 5b, is generated using a method similar to that described in [27] and is deformed to maximize its overlap with the target segmentation while imposing soft regularization constraints to ensure mesh regularity and validity of medial axis geometry as described in [28]. Figure 5a summarizes these definitions. In brief, the template is generated by co-

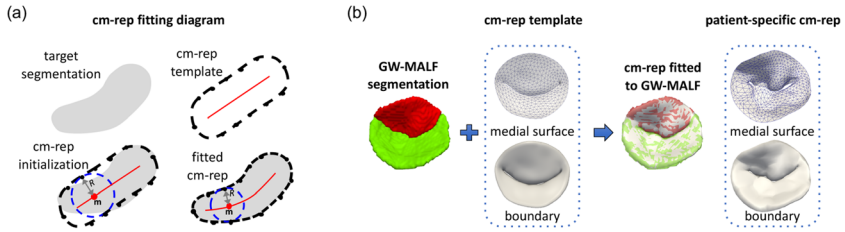

Fig. 5 **a** Overview of continuous medial representation (cm-rep) adapted from [27]. **b** Example of the cm-rep template being fitted to a GW-MALF segmentation in order to generate a patient-specific cm-rep model

registering a population of mitral valve segmentations to generate a unbiased template segmentation that is then manually meshed as described in [27]. The resulting triangulated template is used to model the mitral valve in each 3D frame in each data series.

Kalman Filtering Dynamic measurements derived from cm-reps that are independently fitted to each frame in the output GW-MALF segmentations are inherently noisy. To impose spatiotemporal smoothness on the model series, a Kalman filter [29] is used to recursively estimate the true state of the system (the valve's configuration and motion), which cannot be observed directly but can be estimated by combining noisy observations with the predictions of kinematic equations. Let $\mathbf{x}_t$ denote the true system state at time t and let $\hat{\mathbf{x}}_{t|t-1}$ be the a priori estimate of the system's state at time t with variance $\mathbf{P}_{t\,|\,t-1}$. The vector $\hat{\mathbf{x}}_{t|t-1}$ is determined by applying kinematic equations to the state estimate at $t-1$. Let $\mathbf{z}_t$ be observations of the system made at time t. The goal of the Kalman filter is to combine the a priori estimate $\hat{\mathbf{x}}_{t|t-1}$ and measurements $\mathbf{z}_t$ to generate an a posteriori prediction of the state at time t, denoted by $\hat{\mathbf{x}}_{t|t}$.

In this work, the sought "true" system state is defined by $\mathbf{x}_t = \left[\begin{smallmatrix} x_t \\ \dot{x}_t \end{smallmatrix}\right]$, where x_t denotes vertex coordinates that comprise the medial surface $\mathbf{m}$ and $\dot{x}_t$ denotes their velocities at time t. We treat the cm-rep models fitted independently to different rt-3DE frames as the noisy observations $\mathbf{z}_t$. With a medial mesh consisting of n_p nodes, the total number of state variables is $n_v = 6n_p$. The recursive filter begins by initializing $\hat{\mathbf{x}}_{0|0} = \mathbf{z}_0$ as the medial node coordinates and velocities of the medial model fitted to the first frame of the rt-3DE series. Its covariance is initialized as $\mathbf{P}_{0|0} = \mathbf{0}_{n_v}$. For each subsequent frame, the state is predicted to evolve according to $\hat{\mathbf{x}}_{t|t-1} = \mathbf{F}_t\hat{\mathbf{x}}_{t-1|t-1} + \mathbf{w}_t$, where $\mathbf{F}_t$ is a transition matrix that displaces the nodes with constant velocity and $\mathbf{w}_t \sim \mathcal{N}(0, \mathbf{Q}_t)$ is zero-mean Gaussian distributed process noise with covariance $\mathbf{Q}_t$. The a priori covariance is updated as $\mathbf{P}_{t|t-1} = \mathbf{F}_t\mathbf{P}_{t-1|t-1}\mathbf{F}_t^T + \mathbf{Q}_t$. Noisy measurements of the state at time t are modeled as $\mathbf{z}_t = \mathbf{H}_t\mathbf{x}_t + \mathbf{v}_t$, where $\mathbf{H}_t$ is the identity matrix $\mathbf{I}_{n_v}$ and $\mathbf{v}_t \sim \mathcal{N}(0, \mathbf{R}_t)$ is zero-mean Gaussian distributed measurement noise with covariance $\mathbf{R}_t$. Assuming that the process noise and measurement errors are uncorrelated, the a posteriori state estimate is given by:

$$\begin{aligned} \hat{\mathbf{x}}_{t|t} &= \hat{\mathbf{x}}_{t|t-1} + \mathbf{K}_t\left(\mathbf{z}_t - \mathbf{H}_t\hat{\mathbf{x}}_{t|t-1}\right) \\ \mathbf{P}_{t|t} &= \mathbf{P}_{t|t-1} - \mathbf{K}_t\mathbf{H}_t\mathbf{P}_{t|t-1} \end{aligned} \tag{1}$$

where $\mathbf{K}_t$ is the Kalman gain defined by $\mathbf{K}_t = \mathbf{P}_{t|t-1}\mathbf{H}_t^{\mathrm{T}}\left(\mathbf{H}_t\mathbf{P}_{t|t-1}\mathbf{H}_t^{\mathrm{T}} + \mathbf{R}_t\right)^{-1}$. In this study, $\mathbf{R}_t = \mathbf{I}_{n_v}$ remains constant over time. Since the state evolution equations assume a constant velocity, which does not accurately reflect the nonlinear motion of the valve, we employ a time-varying process noise covariance that increases in magnitude at t_{trans}, the transition time in the cardiac cycle when the valve opens:

$$\mathbf{Q}_t = \alpha(t)\mathbf{I}_{n_v}, \text{where } \alpha(t) = \begin{matrix} 0.1, & t < t_{trans} \\ 1.0, & t \geq t_{trans} \end{matrix} \tag{2}$$

The time-varying $\mathbf{Q}_t$ allows the model fittings to have a stronger influence on the state estimation when the valve accelerates. Once the Kalman filter is applied to the entire series of medial models, measurements of valve dynamics are computed.

Statistical Analysis To assess the smoothing effect (noise reduction) of the Kalman filter, a cubic polynomial was fitted to each set of dynamic measurements before and after Kalman filtering, and the root mean square residuals between the measurements and the cubic polynomial was calculated. The mean of these residuals was calculated for each patient for each measurement, resulting in two sets of 28 residuals per measurement. A paired Student's t test was used to test whether the difference in residuals before and after Kalman filtering was significant for each measurement. In addition, the absolute percent difference between the measurements before and after filtering was calculated to determine if a smoothing effect is achieved with minimal measurement alteration.

To test for inter-group differences in valve dynamics, an independent t-test was used to compare IMR and control group measurements at each time point of the cardiac cycle. A Dunn-Sidak correction ($\alpha = 0.0014$) was used to account for multiple-hypothesis testing. The testing was performed after interpolation to ensure that an equal number of time points in both the IMR and normal groups were assessed.

Results

Valve segmentation and modeling were evaluated in a leave-one-out experiment using manual image segmentation for comparison. For each target image series, the atlas set for each 3D frame consisted of 10 randomly selected frames from the other 13 subjects' data sets within the same sub-group (normal and IMR). Of these 10 randomly selected frames, 8 were from the same phase of the cardiac cycle as the target image and 2 were from the transition phase. For target images in the transitional phase, the atlases consisted of 1 from systole, 8 transitional, and 1 from diastole. The series of segmentations were updated with one groupwise iteration. A representative segmentation result is shown in Fig. 6, and the Kalman-filtered model fittings for the same dataset are illustrated in a supplemental video file. The accuracy of GW-MALF and model fitting relative to manual tracing for all subjects are given in Table 1. Segmentation accuracy was assessed using the mean boundary error (BE) metric, a symmetric measurement of distances between meshes as defined in [27]. Given two meshed shapes P and Q, the MBE is defined as the average of the distances between the two meshes P and Q and Q and P as follows:

$$MBE = \frac{1}{2}(d(P,Q) + d(Q,P)) \tag{3}$$

The distance between the two meshes is given by:

$$d(P,Q) \cong \frac{1}{A_P} \int_{x \in P} \inf_{y \in Q} \|x - y\| \, dA \tag{4}$$

where x is a point on mesh P and y is a point on mesh Q and A_p is the surface area of mesh P.Table.

Dynamic geometric measurements listed in Table 2 were extracted from (1) cm-reps fitted to the GW-MALF segmentations and (2) cm-reps fitted to the GW-MALF segmentations followed by Kalman filtering. Deformable modeling with cm-rep establishes geometric correspondences across all subjects and across all time points in the rt-3DE images, enabling automatic computation of the same valvular features from all subjects at all frames of the rt-3DE data. Without cm-rep model fitting, the measurements in Table 2 could not be computed from the segmentation results in a straightforward manner. To assess the smoothing effect (noise reduction) of the Kalman filter, a cubic polynomial was fitted to each set of dynamic measurements before and after Kalman filtering, and the residual between the measurements and the cubic polynomial was calculated. To evaluate if noise reduction substantially changed the magnitude of the measurements, the average percent difference between the measurements before and after filtering was calculated (Table 2).

For the normal and IMR subgroups, the septolateral diameter (SLD), intercommissural width (ICW), annular bending angle, annular area, posterior and anterior annular circumferences, and total annular circumference were plotted as a function of time, normalized to the cardiac cycle. Bending angle is a measure of flatness of the mitral annulus, with a larger angle signifying a flatter annulus. Figure 8 shows the IMR measurements in blue and normal valve measurements in red. Early systole measurements of septolateral diameter were significantly different between subgroups ($\alpha = 0.0014$), after Sidak correction for multiple hypothesis testing.

The geometric correspondences established by deformable modeling with cm-rep also enable direct comparison of spatially varying valve features between subjects at different phases of the cardiac cycle. To demonstrate this capability, Fig. 8 illustrates a comparison of leaflet thickness between two different cardiac phases: mid-systole and end-diastole.

Discussion

The proposed 4D mitral valve segmentation pipeline combines the attractive properties of multi-atlas segmentation and deformable medial modeling to create descriptive, quantifiable representations of mitral valve dynamics from rt-3DE images. Exemplified in Fig. 6, the output models are visually consistent with the images throughout the cardiac cycle. In addition, the accuracy metrics presented in Table 1 demonstrate that in each cardiac phase, automated segmentation

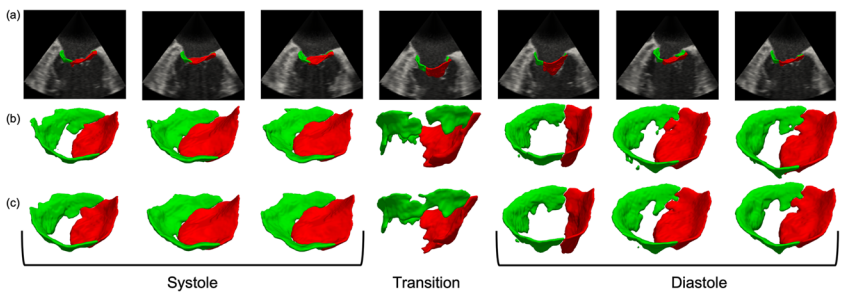

Fig. 6 **a** Manual segmentations overlaid on 3DE slices. **b** MALF results for a subject with ischemic mitral regurgitation. **c** GW-MALF results for the same IMR subject. The anterior leaflet is red and posterior leaflet is green. The cm-rep models fitted to the GW-MALF segmentations in (c) are presented in a supplemental video file

Table 1 Segmentation accuracy based on the symmetric mean boundary error (BE) metric. Mean BE is averaged across all time points within the indicated cardiac phases

	Mean BE (mm)			95th percentile BE (mm)			Max BE (mm)		
	Systole	*Transition*	*Diastole*	*Systole*	*Transition*	*Diastole*	*Systole*	*Transition*	*Diastole*
MALF	0.5 ± 0.2	0.6 ± 0.2	0.6 ± 0.2	1.7 ± 0.9	2.0 ± 0.7	2.0 ± 0.8	4.4 ± 1.8	6.2 ± 2.0	5.5 ± 1.7
GW-MALF	0.4 ± 0.2	0.6 ± 0.2	0.5 ± 0.2	1.6 ± 0.8	2.0 ± 0.7	1.9 ± 0.7	3.8 ± 1.4	5.1 ± 1.9	4.8 ± 1.3
Model fitted to GW-MALF	0.5 ± 0.2	0.7 ± 0.2	0.7 ± 0.2	1.7 ± 0.8	2.2 ± 0.8	2.0 ± 0.8	3.5 ± 1.2	4.5 ± 1.2	4.4 ± 1.1
Kalman-filtered Model*	0.8 ± 0.2	1.2 ± 0.3	0.9 ± 0.2	2.1 ± 0.8	3.1 ± 0.9	2.2 ± 0.7	3.7 ± 1.2	5.2 ± 1.2	4.3 ± 1.1

**Boundary error was calculated by comparing the medial surface of the Kalman-filtered model with the boundary (*i.e., *the atrial and ventricular surfaces) of the manual segmentations, so the BE accounts, in part, for leaflet thickness*

performs on par with user-guided segmentation (0.40 ± 0.32 mm [30]) and compares favorably to other automated 4D segmentation algorithms (0.59 ± 0.49 mm [12] and 1.54 ± 1.17 mm [13]). The pipeline's novelty is its extension of MALF and cm-rep into the spatiotemporal domain by enforcing temporal consistency during both the segmentation and modeling stages. From Table 1, even a single iteration of GW-MALF shows improvement in the quality of multi-atlas segmentations, especially with respect to the mean BE during systole and diastole, as well as the maximum BE. The improvement in temporal consistency of the segmentations is also visually observed in Fig. 6, where GW-MALF can be seen to reduce artifacts in the posterior leaflet. Kalman-filtered cm-reps produce dynamic measurements that are less noisy than those fitted directly to GW-MALF segmentations. This observation is supported by the low p values ($p < 10^{-6}$) reported in Table 2. Moreover, the low percent differences between the measurements computed before and after Kalman filtering suggest that the noise reduction does not substantially change the magnitude of the measurements.

Another important observation in this study is the identification of differences in valve dynamics in patients with normal mitral valve function and in patients with severe IMR. Overall, the dynamics of annular area are consistent with some of the early sonomicrometry ovine studies that described annular dilation at diastole [31]. Figure 7 demonstrates differences in annular dynamics in the normal and IMR subgroups. Increased septolateral diameter and annular bending angle in IMR patients suggest annular dilatation and flattening, which are common features of IMR. Moreover, Fig. 7 suggests that annular dynamics, particularly changes in septolateral diameter, annular area, and annular circumference, may be less pronounced over the cardiac cycle in IMR patients relative to normal mitral valves. Interestingly, this may be due to differing dynamics in the posterior annulus of the IMR and normal subgroups during systole. While the anterior and posterior annular segments of normal mitral valves increase in length over the cardiac cycle (Fig. 7g), the posterior annular segment decreases in length during diastole in the IMR subgroup. In addition to annular dynamics assessment, the image analysis method is able to measure regional leaflet velocities. The free edges of the leaflet were divided into 6 scallops corresponding to the A1, A2, A3, P1, P2, and P3 Carpentier segments, and the average velocity of each segment was calculated over the cardiac cycle. As observed for all leaflet segments, Fig. 7 demonstrates that velocities of the free edge of the A3 and P3 segments rapidly increase with valve opening during diastole. While this behavior seems to be similar for both normal and IMR patients, increasing the number of patients may yield interesting finding regarding especially when stratifying the

Table 2 Root mean square residual (RMSR) in dynamic measurements relative to their best-fit cubic polynomials before and after Kalman filtering of the groupwise multi-atlas segmentation (GW) results. The p value refers to comparison of the residuals for each measurement before and after Kalman filtering. The percent difference between the measurements before and after Kalman filtering is reported

Measurement	RMSR (GW Model)	RMSR (GW + Kalman)	p value	% Difference
Septolateral diameter	0.6 ± 0.2 mm	0.5 ± 0.2 mm	3×10^{-8}	0.80 ± 0.3
Intercommissural width	0.7 ± 0.2 mm	0.5 ± 0.2 mm	2×10^{-10}	0.82 ± 0.2
Bending angle	3.6 ± 1.3 deg	2.6 ± 1.2 deg	1×10^{-11}	1.15 ± 0.4
Annular area	21.7 ± 8.0 mm^2	16.4 ± 6.8 mm^2	1×10^{-7}	0.89 ± 0.5
Anterior annular circumference	1.3 ± 0.4 mm	0.9 ± 0.4 mm	1×10^{-10}	1.23 ± 0.4
Posterior annular circumference	2.3 ± 0.5 mm	1.6 ± 0.5 mm	4×10^{-8}	1.12 ± 0.3

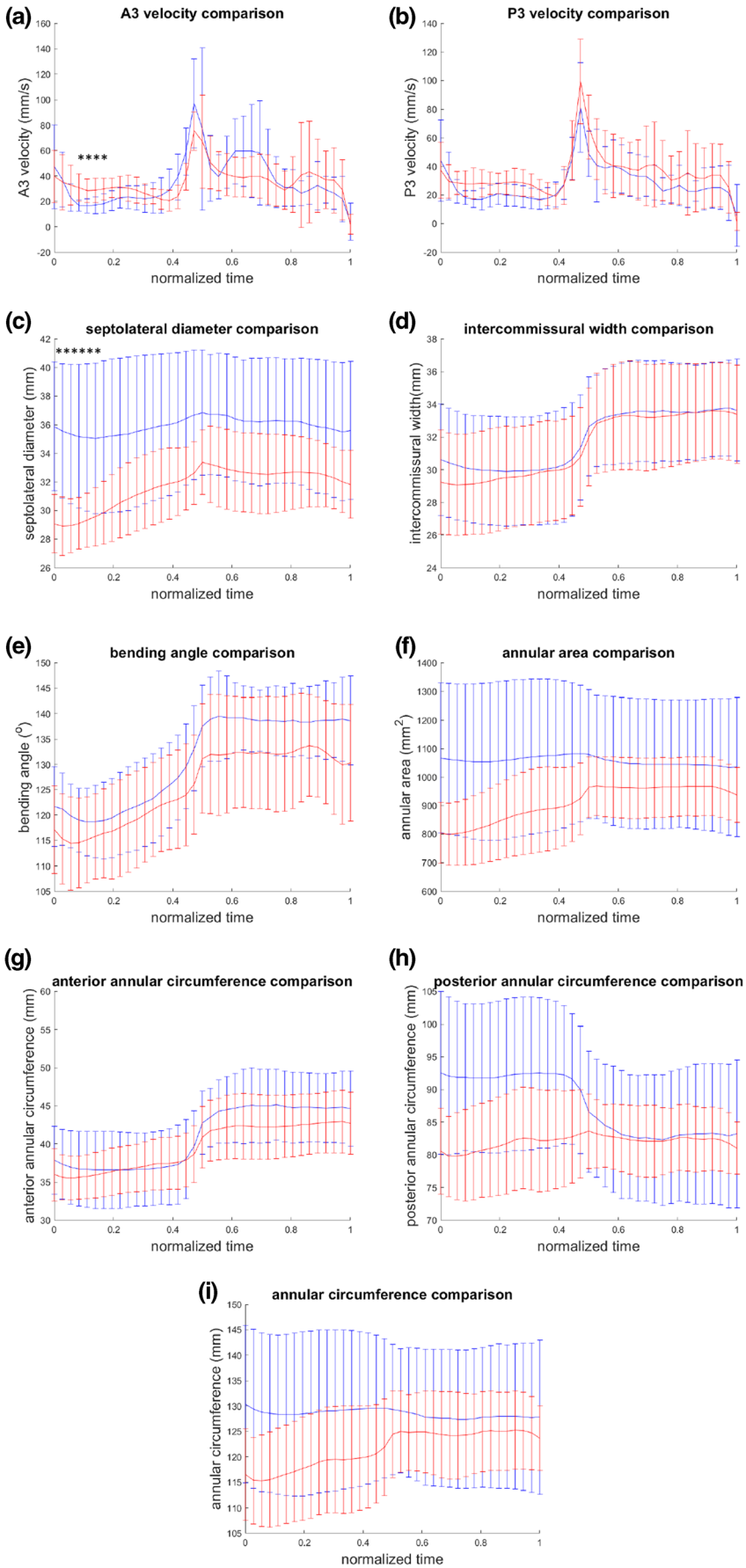

Fig. 7 Comparison of (**a**) A3 leaflet velocity, (**b**) P3 leaflet velocity, (**c**) septolateral diameter (SLD), (**d**) intercommissural width (ICW), (**e**) annular bending angle, (**f**) annular area, (**g**) anterior annular circumference, (**h**) posterior annular circumference, and (**i**) annular circumference in subjects with normal mitral valves (red) and severe IMR (blue) over one cardiac cycle. The error bars represent one standard deviation from the mean. * indicates significant difference between IMR and normal subjects for the given time point

IMR patients based on the pathophysiology of annular dilatation vs leaflet tethering.

For valve mechanics applications, automated image-based segmentation and geometric modeling of the mitral valve over the cardiac cycle can allow for improved, detailed understanding of mitral valve geometry and motion. In particular, the ability to capture regional thickness over time is important for finite element simulations. In a study by Rausch and colleagues [14], finite element simulation was shown to be highly sensitive to parameters such as thickness. Underestimating or overestimating thickness led to different simulated behaviors of the mitral valve leaflets such as larger or smaller deflections of the leaflets into the atrium. Modeling the distribution of thickness is also critical. For example, assuming a uniform thickness distribution overestimates the stiffness of the leaflets towards the free edge and underestimates the stiffness near the annulus [32]. The ability to model thickness throughout the cardiac cycle provides information that can be incorporated into these simulations as well. As seen in Fig. 8, the anterior leaflet appears to be thicker during end diastole when compared to mid systole, suggesting that leaflet stretch may impact leaflet thickness. The ability to capture leaflet velocity is also useful for tissue mechanics simulation by helping to estimate the amount of deflection and restriction of the leaflets. In addition, fluid mechanics and dynamics modeling [33] may have improved accuracy and patient specificity with advanced 4D image-based modeling. It is well known that the anterior leaflet affects vortex formation and transmittal, which in turn reduces energy loss [34]. However, current methods are limited by standardized geometries. Furthermore, the utilization of detailed 4D mitral valve modeling may improve our understanding of how changes in mitral valve dynamics impact cardiac function, and thereby lead to new insight and advancement in surgical and interventional therapies for diseases like mitral regurgitation. For example, a recent study [35] used finite element and fluid structure interaction modeling to demonstrate that the changes in geometry caused by the popular MitraClip procedure may lead to changes in left intraventricular hemodynamics, such as dissipation of the anterior vortex [36] and higher energy loss [37].

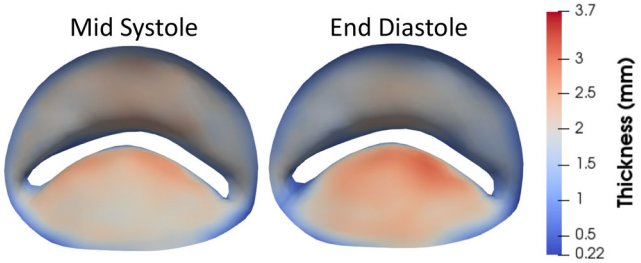

Fig. 8 Mean thickness maps for all subjects combining the normal and IMR subgroups at mid-systole and end-diastole, demonstrating the ability to compare geometric features across time points by using continuous medial axis-based representations. Areas of greater of thickness are indicated in dark red

While the proposed pipeline only requires manual identification of two key frames in the cardiac cycle and five valve landmarks at mid-systole, future work will focus on full automation of the algorithm. In this study, the use of a Kalman filter with a constant velocity model and time-varying process noise provide meaningful time series smoothing. A physical model that better captures the valve's non-linear dynamics could further improve temporal coherence in the output 4D model. Finally, although differing trends in annular dynamics and spatially varying leaflet thickness can be appreciated in the normal and IMR subgroups in Figs. 7 and 8, a larger patient population is needed to verify these interesting findings. The development of this 4D automated segmentation and modeling tool is a step towards better understanding the functional mechanisms underlying IMR progression and post-operative disease recurrence, and can provide patient-specific input to biomechanical simulations that guide surgical simulation and decision making.

Conclusions

Automatic 4D segmentation and modeling allow for reliable physiological, non-invasive reconstruction of the mitral valve over the cardiac cycle. This study demonstrates its application to comparison of mitral annular and leaflet dynamics in pathological and normal mitral valves. The method may help inform finite element modeling by decreasing assumptions about input parameters related to regional mitral valve thickness, geometry, and motion. Future studies can apply this algorithm to a range of cardiovascular mechanics applications, including patient-specific strain estimation, fluid dynamics simulation, inverse finite element analysis, risk stratification of surgical treatment, and development of minimally invasive therapies for valve disease.

Acknowledgements This research was supported by the National Institutes of Health: EB017255 from the National Institute of Biomedical Imaging and Bioengineering, HL073021, HL142504, HL103723, HL141643, and HL142138 from the National Heart Lung and Blood Institute.

Author's Contribution All authors contributed to the study conception and design and have approved the final manuscript. The collection and analysis of human image data was approved by the Institutional Review Board at the University of Pennsylvania.

Compliance with Ethical Standards

Conflict of Interest The authors declare that they have no conflict of interest.

References

1. Krishnamurthy G, Itoh A, Bothe W, Swanson JC, Kuhl E, Karlsson M, Craig Miller D, Ingels NB Jr (2009) Stress-strain behavior of mitral valve leaflets in the beating ovine heart. J Biomech 42(12): 1909–1916. https://doi.org/10.1016/j.jbiomech.2009.05.018
2. Gorman JH 3rd, Gupta KB, Streicher JT, Gorman RC, Jackson BM, Ratcliffe MB, Bogen DK, Edmunds LH Jr (1996) Dynamic three-dimensional imaging of the mitral valve and left ventricle by rapid sonomicrometry array localization. J Thorac Cardiovasc Surg 112(3):712–726
3. Bothe W, Schubert H, Diab M, Faerber G, Bettag C, Jiang X, Fischer MS, Denzler J, Doenst T (2016) Fully automated tracking of cardiac structures using radiopaque markers and high-frequency videofluoroscopy in an *in vivo* ovine model: from three-dimensional marker coordinates to quantitative analyses. Springerplus 5:220. https://doi.org/10.1186/s40064-016-1868-3
4. Zekry SB, Lawrie G, Little S, Zoghbi W, Freeman J, Jajoo A, Jain S, He J, Martynenko A, Azencott R (2012) Comparitive evaluation of mitral valve strain by deformation tracking in 3D-echocardiography. Cardiovasc Eng Technol 3(4):402–412
5. Rego BV, Khalighi AH, Drach A, Lai EK, Pouch AM, Gorman RC, Gorman JH 3rd, Sacks MS (2018) A noninvasive method for the determination of *in vivo* mitral valve leaflet strains. Int J Numer Method Biomed Eng 34(12):e3142. https://doi.org/10.1002/cnm.3142
6. Wang Q, Sun W (2013) Finite element modeling of mitral valve dynamic deformation using patient-specific multi-slices computed tomography scans. Ann Biomed Eng 41(1):142–153
7. Choi A, Rim Y, Mun JS, Kim H (2014) A novel finite element-based patient-specific mitral valve repair: virtual ring annuloplasty. Biomed Mater Eng 24(1):341–347. https://doi.org/10.3233/BME-130816
8. Hammer PE, Perrin DP, del Nido PJ, Howe RD (2008). Image-based mass-spring model of mitral valve closure for surgical planning. PRoceedings of SPIE medical imaging: visualization, image-guided procedures, and modeling 6918
9. Wenk JF, Zhang Z, Cheng G, Malhotra D, Acevedo-Bolton G, Burger M, Suzuki T, Saloner DA, Wallace AW, Guccione JM, Ratcliffe MB (2010) First finite element model of the left ventricle with mitral valve: insights into ischemic mitral regurgitation. Ann Thorac Surg 89(5):1546–1553. https://doi.org/10.1016/j.athoracsur.2010.02.036
10. Ge L, Morrel WG, Ward A, Mishra R, Zhang Z, Guccione JM, Grossi EA, Ratcliffe MB (2014) Measurement of mitral leaflet and annular geometry and stress after repair of posterior leaflet prolapse: virtual repair using a patient-specific finite element simulation. Ann Thorac Surg 97(5):1496–1503. https://doi.org/10.1016/j.athoracsur.2013.12.036
11. Mansi T, Voigt I, Georgescu B, Zheng X, Mengue EA, Hackl M, Ionasec RI, Noack T, Seeburger J, Comaniciu D (2012) An integrated framework for finite-element modeling of mitral valve biomechanics from medical images: application to MitralClip intervention planning. Med Image Anal 16:1330–1346. https://doi.org/10.1016/j.media.2012.05.009
12. Schneider RJ, Tenenholtz NA, Perrin DP, Marx GR, del Nido PJ, Howe RD (2011) Patient-specific mitral leaflet segmentation from 4D ultrasound. Med Image Comput Comput Assist Interv 14(Pt 3): 520–527
13. Ionasec RI, Voigt I, Georgescu B, Wang Y, Houle H, Vega-Higuera F, Navab N, Comaniciu D (2010) Patient-specific modeling and quantification of the aortic and mitral valves from 4-D cardiac CT and TEE. IEEE Trans Med Imaging 29(9):1636–1651. https://doi.org/10.1109/TMI.2010.2048756
14. Rausch MK, Famaey N, Shultz TO, Bothe W, Miller DC, Kuhl E (2012) Mechanics of the mitral valve : a critical review, an *in vivo* parameter identification, and the effect of prestrain. Biomech Model Mechanobiol 12:1053–1071. https://doi.org/10.1007/s10237-012-0462-z
15. Acker MA, Parides MK, Perrault LP, Moskowitz AJ, Gelijns AC, Voisine P, Smith PK, Hung JW, Blackstone EH, Puskas JD, Argenziano M, Gammie JS, Mack M, Ascheim DD, Bagiella E, Moquete EG, Ferguson TB, Horvath KA, Geller NL, Miller MA, Woo YJ, D'Alessandro DA, Ailawadi G, Dagenais F, Gardner TJ, O'Gara PT, Michler RE, Kron IL, Ctsn (2014) Mitral-valve repair versus replacement for severe ischemic mitral regurgitation. N Engl J Med 370(1):23–32. https://doi.org/10.1056/NEJMoa1312808
16. Bouma W, Lai EK, Levack MM, Shang EK, Pouch AM, Eperjesi TJ, Plappert TJ, Yushkevich PA, Mariani MA, Khabbaz KR, Gleason TG, Mahmood F, Acker MA, Woo YJ, Cheung AT, Jackson BM, Gorman JH 3rd, Gorman RC (2016) Preoperative three-dimensional valve analysis predicts recurrent ischemic mitral regurgitation after mitral Annuloplasty. Ann Thorac Surg 101(2): 567–575; discussion 575. https://doi.org/10.1016/j.athoracsur.2015.09.076
17. Pouch AM, Aly AH, Lai EK, Yushkevich N, Stoffers RH, Gorman JH, Cheung AT, Gorman JH 3rd, Gorman RC, Yushkevich PA (2017) Spatiotemporal segmentation and modeling of the mitral valve in real-time 3D echocardiographic images. Med Image Comput Comput Assist Interv 10433:746–754. https://doi.org/10.1007/978-3-319-66182-7_85
18. Yushkevich PA, Piven J, Hazlett HC, Smith RG, Ho S, Gee JC, Gerig G (2006) User-guided 3D active contour segmentation of anatomical structures: significantly improved efficiency and reliability. Neuroimage 31(3):1116–1128. https://doi.org/10.1016/j.neuroimage.2006.01.015
19. Pouch AM, Yushkevich PA, Jackson BM, Jassar AS, Vergnat M, Gorman JH, Gorman RC, Sehgal CM (2012) Development of a semi-automated method for mitral valve modeling with medial axis representation using 3D ultrasound. Med Phys 39(2):933–950
20. Carnahan P, Ginty O, Moore J, Lasso A, Jolley MA, Herz C, Eskandari M, Bainbridge D, Peters TM (2019). Interactive-automatic segmentation and modelling of the mitral valve. In: International Conference on Functional Imaging and Modeling of the Heart. Springer, pp 397–404
21. van Zon M, Veta M, Li S (2019). Automatic cardiac landmark localization by a recurrent neural network. In: Medical Imaging 2019: Image Processing. International Society for Optics and Photonics, p 1094916
22. Avants BB, Epstein CL, Grossman M, Gee JC (2008) Symmetric diffeomorphic image registration with cross-correlation: evaluating automated labeling of elderly and neurodegenerative brain. Med Image Anal 12(1):26–41. https://doi.org/10.1016/j.media.2007.06.004
23. Wang H, Suh JW, Das SR, Pluta JB, Craige C, Yushkevich PA (2012) Multi-atlas segmentation with joint label fusion. IEEE Trans Pattern Anal Mach Intell 35(3):611–623
24. Wang H, Yushkevich PA (2013). Multi-atlas segmentation without registration: a supervoxel-based approach. Paper presented at the Medical Image Computing and Computer Assisted Intervention,
25. Wang H, Yushkevich PA (2013). Groupwise segmentaiton with multi-atlas joint label fusion. Paper presented at the Medical Image Computing and Computer Assisted Intervention
26. Yushkevich PA, Zhang H, Gee JC (2006) Continuous medial representation for anatomical structures. IEEE Trans Med Imaging 25(12):1547–1564
27. Pouch AM, Tian S, Takebe M, Yuan J, Gorman R Jr, Cheung AT, Wang H, Jackson BM, Gorman JH 3rd, Gorman RC, Yushkevich PA (2015) Medially constrained deformable modeling for segmentation of branching medial structures: application to aortic valve

segmentation and morphometry. Med Image Anal 26(1):217–231. https://doi.org/10.1016/j.media.2015.09.003
28. Pouch AM, Wang H, Takabe M, Jackson BM, Gorman JH 3rd, Gorman RC, Yushkevich PA, Sehgal CM (2014) Fully automatic segmentation of the mitral leaflets in 3D transesophageal echocardiographic images using multi-atlas joint label fusion and deformable medial modeling. Med Image Anal 18(1):118–129. https://doi.org/10.1016/j.media.2013.10.001
29. Kalman RE (1960) A new approach to linear filtering and prediction problems. J basic Eng 82(series D):35–45
30. Siefert AW, Icenogle DA, Rabbah JP, Saikrishnan N, Rossignac J, Lerakis S, Yoganathan AP (2013) Accuracy of a mitral valve segmentation method using J-splines for real-time 3D echocardiography data. Ann Biomed Eng 41(6):1258–1268. https://doi.org/10.1007/s10439-013-0784-8
31. Gorman JH III, Gupta KB, Streicher JT, Gorman RC, Jackson BM, Ratcliffe MB, Bogen DK, Edmunds LH Jr (1996) Dynamic three-dimensional imaging of the mitral valve and left ventricle by rapid sonomicrometry array localization. J Thorac Cardiovasc Surg 112(3):712–724
32. Krishnamurthy G, Itoh A, Swanson JC, Bothe W, Karlsson M, Kuhl E, Miller DC, Ingels NB Jr (2009) Regional stiffening of the mitral valve anterior leaflet in the beating ovine heart. J Biomech 42(16):2697–2701
33. Bavo A, Pouch AM, Degroote J, Vierendeels J, Gorman JH, Gorman RC, Segers P (2017) Patient-specific CFD models for intraventricular flow analysis from 3D ultrasound imaging: comparison of three clinical cases. J Biomech 50:144–150
34. Falahatpisheh A, Pahlevan NM, Kheradvar A (2015) Effect of the mitral valve's anterior leaflet on axisymmetry of transmitral vortex ring. Ann Biomed Eng 43(10):2349–2360
35. Caballero A, Mao W, McKay R, Hahn RT, Sun W (2020). A comprehensive engineering analysis of left heart dynamics after MitraClip in a functional mitral regurgitation patient. Front Physiol 11
36. Jeyhani M, Shahriari S, Labrosse M (2018) Experimental investigation of left ventricular flow patterns after percutaneous edge-to-edge mitral valve repair. Artif Organs 42(5):516–524
37. Du D, Jiang S, Wang Z, Hu Y, He Z (2014) Effects of suture position on left ventricular fluid mechanics under mitral valve edge-to-edge repair. Biomed Mater Eng 24(1):155–161

Publisher's Note Springer Nature remains neutral with regard to jurisdictional claims in published maps and institutional affiliations.